QUANTIFYING COASTAL MARSH EROSION USING A LIDAR TERRESTRIAL LASER SCANNER: THE ROLE OF WAVES, SOIL, AND VEGETATION

A Thesis

by

ARTURO DELGADO JR

Submitted to the Office of Graduate and Professional Studies of
Texas A&M University
in partial fulfillment of the requirements for the degree of

MASTER OF SCIENCE

Chair of Committee,	Rusty Feagin
Committee Members,	Sorin C. Popescu
	Chris Houser
Head of Department,	Kathleen Kavanagh

August 2016

Major Subject: Ecosystem Science and Management

ABSTRACT

Coastal marshes on the Gulf Coast of Texas are an important transition zone between the ocean and land, acting as an ecological buffer and providing invaluable ecosystem services to people and the surrounding environment. Accelerated erosion threatens the stability of these regions and a greater understanding of the interacting processes is vital to the preservation of coastal marshes.

The central objective of this study is to evaluate the impacts of wave energy, vegetation, and soil properties on coastal marsh edge erosion. To accomplish this, the first objective was to quantify tidal marsh edge erosion across temporal and spatial scales using TLS. The second objective was to evaluate the relationships between marsh edge erosion and incident wave energy. The final objective was to assess the correlation between vegetation roots and marsh edge erosion as well as the correlation between soil properties and marsh edge erosion.

The study area is on an eroding edge of a salt marsh wetland known as Anchor Bay, located at the terrestrial-aquatic interface of Galveston Island and West Bay specifically, between Melager Cove and Oxen Bayou. Galveston Island is a barrier island on the Texas Gulf Coast, located about 50 miles southeast of Houston, Texas, U.S.A.

Many methods were used to accomplish the objectives including LiDAR and photographic surveying, point cloud change analysis, wave modeling, image

classification and soil analysis for bulk density, percent organic matter, and sediment grain size.

Overall, lateral marsh edge erosion at the study site for the duration of the study was relatively large with greater than 1 meter of erosion observed at the study site in a 318 day period. Wave heights, as driven by wind direction and speed, affected the erosion at the study site. The site was prone to greater erosion when winds blew from the east-northeast to the north directions, and from the north-northwest to the west directions. While root concentration did not play an apparent role in preventing erosion, soil properties did have some influence on erosion.

DEDICATION

To Delta and Dallas and the memories they made on Galveston Island

ACKNOWLEDGEMENTS

I would like to thank my committee chair, Dr. Feagin, for his continual guidance, leadership, and support through the course of this research. Also, much thanks to my committee members, Dr. Popescu and Dr. Houser, for their direction and teachings which were always very valuable. Thank you also to Dr. Popescu and his lab for the use of his TLS equipment and all the additional technical support.

Thank you also to my friend and colleague, Thomas Huff, for his constant help with my research from writing scripts to ease analysis to help conducting field research and making every trip to Galveston a great experience.

I would like to thank my wife, Marie, for being my rock throughout this process. My education would not have been possible if it was not for your constant support and encouragement. I cannot express how grateful I am for having you by my side every step of the way through this work and in life.

CONTRIBUTORS AND FUNDING SOURCES

This work was supported by a thesis committee consisting of Professor Rusty Feagin, serving as advisor, and Professor Sorin Popescu of the Department of Ecosystem Science and Management, and Professor Chris Houser of the Department of Geography.

The analyses depicted in Section 3 were conducted in part by Thomas Huff of the Department of Ecosystem Science and Management.

All other work conducted for the thesis was completed by the student independently.

This thesis was made possible in part by an Institutional Grant (NA14AR4170102) to the Texas Sea Grant College Program from the National Sea Grant Office, National Oceanic and Atmospheric Administration, U.S. Department of Commerce. Its contents are solely the responsibility of the authors and do not necessarily represent the official views of the National Oceanic and Atmospheric Administration.

NOMENCLATURE

LiDAR	Light Detection and Ranging
C2C	Cloud-to-Cloud
M3C2	Multiscale Model to Model Cloud Comparison
WDG	Wind Direction Group
TLS	Terrestrial Laser Scanner
3D	3 Dimensional
2D	2 Dimensional
HMLS	Handheld Mobile Laser Scanning
DTM	Digital Terrain Model
DSM	Digital Surface Model
CHM	Canopy Height Model
LOI	Lost On Ignition
ROI	Regions Of Interest
RGB	Red Green Blue
MPH	Miles Per Hour
RMS	Root Mean Square

TABLE OF CONTENTS

Page

LIST OF FIGURES

Page

LIST OF TABLES

Page

1. INTRODUCTION

Coastal marshes on the Gulf Coast of Texas are an important transition zone between the ocean and land. Marshes provide invaluable ecosystem services to people and the surrounding environment; services including carbon sequestration, acting as fish hatcheries, filtering nutrients and pollution from the water for improved water quality, and flood protection from rising sea levels and harsh storms. Accelerated erosion threatens the stability of these regions and the loss of these ecosystems would have significant negative impacts. A greater understanding of the interacting processes is vital to the preservation of coastal marshes.

Because of their orientation on the coast, marshes are subjected to hurricanes, tropical storms, cold front systems, and other severe weather events that increase wave action and cause erosion along their edges. Hurricanes are historically common on the Gulf Coast of Texas, with the frequency of hurricanes along any 80 km stretch of the coast occurring once every 6 years [*Roth,* 2010]. Cold front systems are normally occurring weather patterns for the area, with multiple instances occurring yearly. Wind generated waves from strong fronts and tropical storms have been identified as responsible for the deterioration of salt marshes [*Houser,* 2010].

Marsh plants, such as *Spartina alterniflora,* are adapted to the salt water environment and to water levels that fluctuate with tide. *Spartina alterniflora* spreads by means of a subterranean rhizome system and grows densely encouraging sedimentation of organic matter. Marsh vegetation, such as this, may be capable of holding soil in

place with their root systems and absorbing energy generated from wave impacts, but there has been little research conducted on this topic in the field.

Terrestrial Laser Scanning (TLS) is an established method for obtaining 3D data rapidly and accurately at small scales. By collecting multiple datasets over time at a specific area of interest, change detection analysis of the obtained point clouds can demonstrate changes with fine scale models and aid scientists in calculating rates of change. Further, the use of soil analysis techniques, such as the quantification of bulk density and percent organic matter, are proven techniques for identifying soil profiles to assess the resilience and stability of an ecosystem and it's resistance to erosion.

The central objective of this study was to evaluate the impacts of wave energy, vegetation, and soil properties on coastal marsh edge erosion. To accomplish this, the first objective was to quantify tidal marsh edge erosion across temporal and spatial scales using TLS. The second objective was to evaluate the relationships between marsh edge erosion and incident wave energy. The final objective was to assess the correlation between vegetation roots and marsh edge erosion as well as the correlation between soil properties and marsh edge erosion.

Erosion can be caused by many factors. We aimed to evaluate the impact of wave energy on marsh edge erosion and the ability of the vegetation and soil properties to mediate erosion. To accomplish this we quantified the erosion and wave energy occurring in situ for 318 days and evaluated the vegetation and soil characteristics of the site.

2. LITERATURE REVIEW

Coastal marshes on the Gulf Coast of Texas provide vital ecosystem services to people and the environment ranging from flood protection and erosion control to carbon sequestration and water purification. Coastal zones are in a constant state of physical and geological flux caused by tidal activity, sea level rise, and high energy events such as strong storms. Salt marshes exist within these zones and are some of the richest ecosystems in terms of species diversity and productivity [e.g. *Teal*, 1962; *van der Wal and Pye*, 2004].

Multiple studies have evaluated the coastal marshes of Galveston Bay and the influencing factors on shoreline change. From 1950 to 1989, Galveston Bay experienced both gains and losses to wetlands habitats with an overall trend of wetland loss amounting to 19% [*White* et al., 1993]. Between 1930 and 1994, about 9% of Galveston Island State Park was lost [*Glass and Hollingsworth*, 1999]. Gibeaut et al. [2003] indicated that Galveston's West Bay system experiences 48% retreat, 47% stability, and 6% advancement, with an average rate of change of -0.88 m/yr since 1930. Losses are attributed to human-induced subsidence, relative sea-level rise, and development pressures, as well as the conversion of wetlands to open water and barren flats [*White* et al., 1993]. Salt marsh losses from fault-induced subsidence resulting from hydrocarbon production are also documented [*White and Morton*, 1997]. Additional influences to wetland loss which have been recognized include loss of fluvial sediment supply and coastal subsidence [*White* et al., 2002]. Though relative sea-level rise may play a role,

erosion by waves and currents have also impacted coastal erosion in Galveston Bay as well [*Gibeaut* et al., 2003].

Many conflicting study results exist regarding the influence of wave action on rates of marsh erosion. Wind speed, wind direction, wind occurrence, fetch distance, and water depth are factors in wave climate at a given location [*Fagherazzi and Wiberg* 2009]. Wave height and water level is of great importance in determining rates of erosion, as over wash is a strong contributor to erosion and accretion dynamics [*Hackney* et al., 2015]. Wave generated erosion has been identified as a main contributor to salt marsh loss [*Leonardi and Fagherazzi*, 2014]. Shafer et al. [2003] have shown wave action to be a cause of marsh erosion in Galveston Bay, and Houser [2010] demonstrates that generated wind waves during strong frontal or tropical storms are responsible for the deterioration of salt marshes. Wave heights that exceed the 20^{th} percentile of wave conditions have a greater influence on long-term shoreline stability causing marshes to suffer from erosion due to wave action [*Shafer* et al., 2003]. In West Galveston Bay salt marshes, if the 20% exceedance wave height is less than 0.17 m, the marsh erosion rate was shown to not be effected by wave-induced erosion and further conclusions conclude that marsh loss in West Galveston Bay is more likely a result of the low sedimentation accretion rate (0.20 cm year $^{-1}$) relative to the relative sea-level rise rate (0.65 cm year $^{-1}$) [*Ravens* et al., 2009]. In contrast, Gibeaut et al. [2003] found that small, sheltered bays had less shoreline retreat implicating exposure to wave energy as a cause. Further studies have concluded a linear relationship between wave energy and lateral rates of shoreline retreat [e.g. *Marani* et al., 2011; *Leonardi* et al., 2016; *Schwimmer*, 2001]. Margin lateral

erosion has been identified as a primary mechanism leading to marsh loss and the rate of volumetric margin retreat and linear margin retreat have been independently shown to be related to the mean annual wave power density [*Marani* et al., 2011]. A linear relationship exists where salt marsh retreat still occurs regardless of how low wave energy conditions become as a threshold below which no erosion would be expected does not exist [*Leonardi* et al., 2016]. Furthermore, as wave energy increases, salt marshes do not retreat exponentially, emphasizing the resilience of salt marshes against extreme events, because of their short duration [*Leonardi* et al., 2016]. The greatest contributor to salt marsh retreat is moderate, regularly occurring weather conditions [*Leonardi* et al., 2016].

Past salt marsh eco-geomorphology work has focused primarily on accretion and biotic control of long-term sedimentary processes. Coastal morphodynamic studies tend to be focused on studies at localized scales which do not contribute to fundamental knowledge on nearshore hydrodynamics and sediment transport [*French and Burningham,* 2009]. Ravens et al. [2009] has suggested that the variability of marsh erosion rates is probably due to variability in the gap between sediment accretion rate and relative sea-level rise. A long-term average sedimentation rate of Texas coastal drainage basins was measured at 0.5 cm year $^{-1}$ in conjunction with a local relative seal-level rise rate of 1.1 cm year $^{-1}$ [*White* et al., 2002].

Physical erosion is a different process, operating at much finer spatial and temporal scales. Aboveground portions of vegetation generally attenuate flow and waves, but there has been little work on the ability of roots to mediate wetland edge

erosion, a belowground process. Feagin et al. [2009] addressed the belowground process and found that roots are not reducing wave erosion in a direct sense at fine scales, but Silliman et al. [2012] suggest that aggregated mats of roots may reduce erosion at coarser spatial and temporal scales. Francalanci et al. [2013] further explain that tension cracks, overhanging profiles, and mean bank-height water level are all factors that make a salt marsh more susceptible to erosion by wave impact; however, adequate roots did delay mass failures.

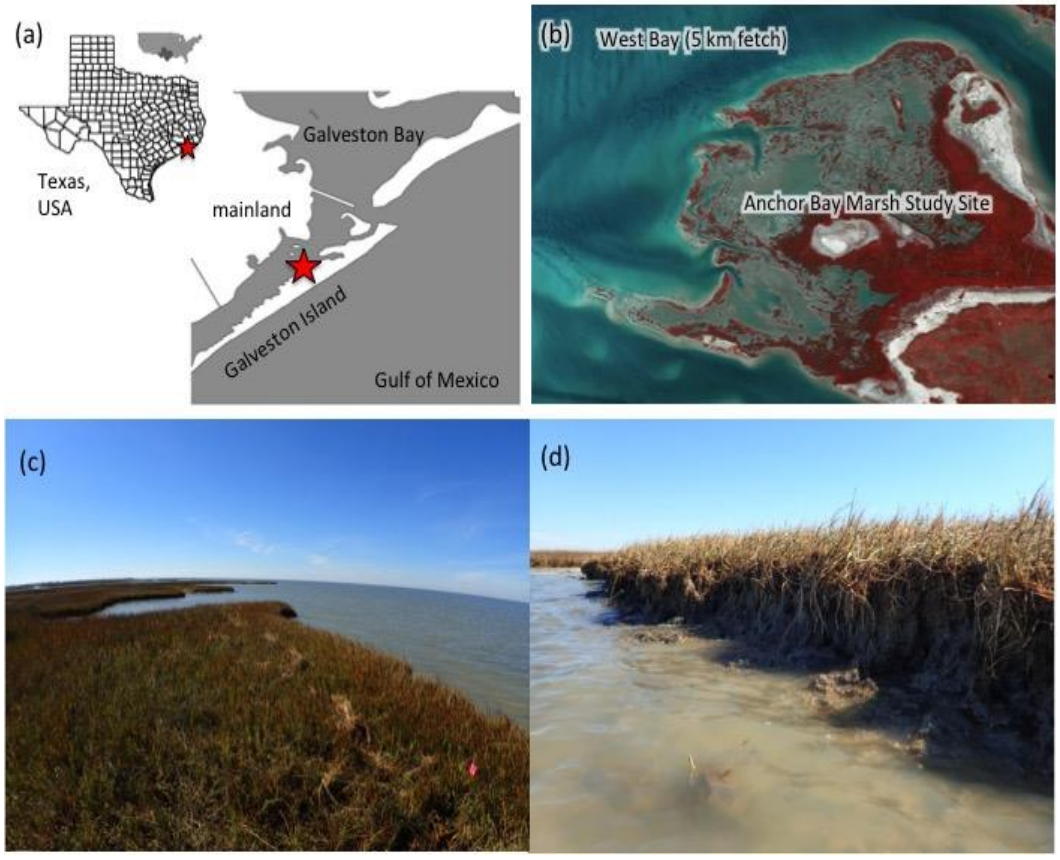

Figure 1. a) Location of the marsh area study site in relation to its location on Galveston Island, Texas. b) False color composite aerial imagery of the marsh study site in Anchor Bay. c) and d) Photos of the marsh study site taken on February 26, 2015.

3. METHODS

3.1 Terrestrial LIDAR Scanning to Quantify Tidal Marsh Edge Erosion across Temporal and Spatial Scales

3.1.1 Study Area

The study area is on an eroding edge of a salt marsh wetland known as Anchor Bay, located at the terrestrial-aquatic interface of Galveston Island and West Bay (Figure 1). Specifically, the site is located between Melager Cove and Oxen Bayou. Galveston Island is a barrier island on the Texas Gulf Coast, located about 50 miles southeast of Houston, Texas, U.S.A. The island stretches 27 miles long by 3 miles wide at its widest point. The island is oriented northeast-southwest, with the Gulf of Mexico bordering on the east and south, West Bay on the west, and Galveston Bay towards the north. The study site is approximately 3.80 km SE of 8 Mile Road, which provides public access to West Bay for recreational use.

3.1.2 TLS Overview

TLS is a ground-based, 3D imaging technology that rapidly acquires accurate positions of object surfaces by laser range finding. The application of TLS instruments to remote sensing varies from urban planning and archeology to ecological assessments such as forest surveys, vegetation analysis, change detection, erosion analysis, and topographic surveys. TLS shows promise for unbiased and reliable forest metric assessments, such as stem location, tree height, diameter at breast height, stem density, and timber volume [*Hopkinson* et al., 2004] and newer technologies like handheld

mobile laser scanning (HMLS) are proving to contribute to the benefits of forest surveying with TLS by contributing to success rates and techniques [*Ryding* et al., 2015]. TLS developments have also contributed to the ability to study vegetation density characteristics. Pirotti et al. [2011] constructed a method which utilizes a typical TLS dataset and produces a Digital Terrain Model (DTM), a Digital Surface Model (DSM), a vegetation density map, and a derived canopy height model (CHM) with minimal user interaction and consistent results using traditional methods. TLS also provides the ability to compute change detection over time. Many methods have been tested to conduct change detection; certain methods provide better accuracy for specific scanning circumstances such as shorter temporal scale, longer temporal scale, surface roughness, and scan registration [*Barnhart and Crosby*, 2013].

TLS has contributed to coastal analysis applications in multiple ways despite the many obstacles natural coastal environments present. Seacliff erosion presents a difficult situation, but georeferenced TLS datasets have made it possible to conduct reliable comparisons of time-series surveys to quantify change in cliff location and geometry [*Olsen* et al., 2009]. The use of high-resolution TLS in marsh areas with low relief aids in the creation of high-resolution and high-accuracy DTMs and DSMs, which provide fair portrayals of marsh morphology [*Guarnieri* et al., 2009]. Similarly, TLS has proven beneficial when evaluating anthropogenic beach berm dynamics and the impact on coastal flooding by providing base data for use in models for predicting beach berm erosion and wave overtopping [*Schubert* et al., 2015].

TLS is suitable for surveying in the highly-dynamic coastal environment as it is optimal for monitoring changes at multiple temporal scales and other field methods may be too time consuming. For example, beach morphology can be dynamic, but TLS is effective at monitoring and evaluating beach change in short time intervals, providing the ability to analyze sediment volume changes [*Silva dos Santos* et al., 2014]. Additionally, TLS has been leveraged to calculate accurate volumes of dislocated boulders moved by high-energy coastal activity as well as monitoring annual changes in coastal characteristics [*Hoffmeister* et al., 2012]. Still, despite the benefits of using TLS to quantify geomorphic changes, the size of a TLS dataset should be considered as it can have a direct effect on the post-processing computation times. For the positives to be worthwhile, point cloud registration, resolution, and interpolation errors should be strongly considered during project design [*Feagin* et al., 2014].

3.1.3 TLS and Photographic Data Acquisition

LiDAR data was acquired using a Leica ScanStation 2 TLS (Leica Geosystems AG, Heerburgg, St. Gallen, Switzerland, ScanStation 2). For consistent scans and to minimize georeferencing errors, benchmarks and reflective targets were placed for the TLS system. Benchmarks were constructed following standard USGS methods for unconsolidated marshes [*Cahoon* et al., 2003]. Each reflective target benchmark was positioned approximately 3 m from the marsh edge on top of each benchmark. To further mark the extent of the study area, survey stakes and PVC pipes were placed on the left and right outer edge of the site boundary.

For all scans, scan point spacing resolution was set to 0.02 m horizontal and 0.02 m vertical at a range of 15 m (actual point density was greater due to the range of approximately 8 m to the initial edge location). Scans were performed only during relatively low tide conditions that exposed the marsh edge. The TLS was mounted on a survey tripod at a benchmark located 8 m offshore from the edge. Upon acquiring the reflective targets, a fence was created in Leica's Cyclone software and the scan was conducted. Co-located, high-resolution photographic images also were collected during each scan. The point cloud, along with the referenced imagery values, were then imported into CloudCompare 2.6.1 for cloud registration and analysis.

The study site was first surveyed on February 26, 2015. Comparative surveys were conducted on March 06, 2015, April 30, 2015, and January 10, 2016 following cold weather events. An additional comparative scan was conducted on August 24, 2015 following Hurricane Bill, which occurred on June 16, 2015.

3.1.4 TLS Data Analysis

TLS data analysis was conducted using CloudCompare 2.6.1. TLS point cloud datasets were imported into CloudCompare and then co-registered to the first dataset using a point pairs picking method. In order to obtain the lowest root mean square value (RMS), a minimum of four points were selected from each point cloud for registration. For consistency, the reflective targets and survey stakes were utilized for point pairs picking. A transformation matrix was then applied to each point cloud. The marsh edge profile was then segmented to remove any points from the registered point cloud which were not coincident with the marsh edge as well as any points that were associated with

the aboveground portions of vegetation (stems, leaves, flowering portions). The resulting data was analyzed with the Cloud-to-Cloud (C2C) algorithm and Multiscale Model to Model Cloud Comparison (M3C2) algorithm.

3.1.5 C2C Analysis

The C2C algorithm is a user-friendly 3D comparison method of point cloud data. It does not require significant parameter settings to run the algorithm, such as gridding or meshing of point clouds and calculating surface normals. Input point clouds are described as a reference (R_c) dataset or a compared (C_c) dataset. Using each point from the compared cloud and finding the closest point in the reference cloud, the distance between datasets is calculated. Surface change is estimated by calculating the distance between the two point cloud datasets. For complex datasets, additional local modeling parameters, such as the height function, 2D ½ triangulation, and least square plane, are available to be applied to the reference model [*Lague* et al., 2013]. CloudCompare has the ability to analyze the overall distance between two point clouds as well as splitting the computed distances along the x, y, and z planes.

A C2C point cloud analysis was conducted utilizing the point cloud acquired on February 26, 2015 as the reference dataset. The point clouds acquired on March 06, 2015, April 30, 2015, August 24, 2015, and January 10, 2016 were used as the comparative datasets. The resulting produced 4 interval change detection datasets which show the change from erosion loss in meters – interval 1 (February to March), interval 2 (February to April), interval 3 (February to August), and interval 4 (February to January). Additionally, each interval's computed distances were split along the x, y, and

z planes producing east-west, north-south, and vertical distance change from erosion loss.

3.1.6 M3C2 Analysis

Rapid analysis of point clouds in complex 3D environments can be done through the use of the M3C2 algorithm. This algorithm does not require the use of point cloud gridding or meshing to conduct analysis on point cloud datasets. M3C2 is able to detect surface orientation in 3D space by computing the local distances between two point clouds along a normal surface orientation [*Lauge* et al., 2013].

The M3C2 algorithm uses point normal estimation to conduct surface change analysis and can be defined as having 2 primary steps – calculation of normals and calculation of the average distance between the point clouds. Local point cloud normals can be calculated or fixed in the vertical or horizontal position. M3C2 speeds up calculations of dense point clouds by utilizing core points, which are a subset of the reference point cloud [*Lague* et al., 2013]. The algorithm requires two user-defined parameters – normal scale (*D*) and projection scale (*d*). Normal scale should be based on density and roughness of the reference point cloud [*Barnhart and Crosby,* 2013]. Projection scale is used to calculate the distances between two point clouds and is determined by the defined radius and length of a projection cylinder. Once the normal is defined for a core point, it projects the point onto each cloud at the projection scale by defining the average position of points in the vicinity for each dataset. Both datasets exist inside the projection cylinder and are spatially averaged to calculate the mean surface positions of points along the normal direction [*Lague* et al., 2013].

A M3C2 point cloud analysis was conducted utilizing the point cloud acquired on February 26, 2015 as the reference dataset. The point clouds acquired on March 06, 2015, April 30, 2015, August 24, 2015, and January 10, 2016 were used as the comparative datasets. The resulting produced 4 interval change detection datasets which show the change from erosion loss in meters – interval 1 (February to March), interval 2 (February to April), interval 3 (February to August), and interval 4 (February to January). For analysis of each interval, the parameters were consistently defined with normal scale as 0.02 m, projection scale as 2.5 m, and maximum cylinder depth as 2.5 m. Total registration errors for the comparative datasets were defined as 0.05 m, 0.12 m, 0.11 m, and 0.04 m, respectively. Point cloud normals were fixed in the horizontal direction and core point subsets were not utilized.

3.2 Correlating Marsh Edge Erosion with Incident Wave Energy

3.2.1 Wave Sensor Model

To determine the incident wave energy impacting the study site, an ultrasonic wave sensor was placed in the marsh for a span of 9 days (December 10 to December 18, 2015). The wave sensor sampled at 20 hz. During this time period, a large range of sea state conditions were encountered, with wind occurring from every direction and speeds ranging from 3.5 mph to 24.2 mph, arising across a maximum fetch of approximately 6.25 km. A custom script in R Studio 2.1 was used to convert the collected data from voltage (as recorded by the sensor) to centimeters. For each 2-hour interval of data collected, a 1-minute subset was extracted for analysis. A total of 118 1-minute subsets, each containing 1200 data points, were extracted and compiled.

MATLAB was then utilized to smooth noise and data spikes using the 3D phase space method proposed by Mori, Suzuki and Kakuno [2007]. The 9-day time series of collected wave heights were input and the first and second derivatives were calculated. Next, the universal threshold was calculated from the number of data collected and the correlation between wave height and the second derivative of wave height was also calculated. The algorithm then produces an inclined ellipsoid of wind speed, the first derivative, and the second derivative with the angle calculated from the correlation between wind speed and the second derivative. The major and minor axes of the ellipsoid are determined as the universal threshold of wind speed, the universal threshold of the first derivative, and the universal threshold of the second derivative. The points that lie outside of the ellipsoid are then identified and replaced. The process is repeated until spikes are no longer detected.

Further analysis was conducted using the Ocean Wave Analyzing Toolbox in MATLAB as detailed by Karimpour [2015]. The despiked wave height data was input into the wave spectral function. Other inputs needed for the analysis included the sampling frequency, duration of data collection, and sensor height from bed. These inputs were used to calculate wave properties utilizing the wave surface elevation power spectral density producing significant wave height (Hm0), wave frequency (Tp), and wave period (fp).

Hourly temperature, wind speed, and wind direction data for the study site was acquired from the Scholes International weather station in Galveston ("Weather History for Galveston, TX."), for dates ranging from February 26, 2015 to January 10, 2016.

This weather station is approximately 7.3 km distance from the wave sensor location. Wave energy data collected by the sonic wave sensor was co-referenced according to time with the hourly weather data to analyze the relationship between significant wave height and wind speed. Wind directional groups were created to investigate the relationship between significant wave height, wind speed, and wind direction. Wind directions were grouped for analysis as follows: wind direction group 1 (WDG 1) includes ENE, NE, NNE and N; wind direction group 2 (WDG 2) includes NNW, NW, WNW, and W; and wind direction group 3 (WDG 3) includes WSW, SW, SSW, S, SSE, SE, ESE, and E.

Regression analysis was conducted on wind speed versus significant wave height for each wind direction group resulting in the following regression equations:

$$y = 1.0056x - 4.1377\ (WDG\ 1)$$

$$y = 0.5699x + 7.4852\ (WDG\ 2)$$

$$y = -0.0133x + 4.3199\ (WDG\ 3)$$

Further regression analysis was conducted on wind speed versus wave frequency, and wind speed versus wave period for each wind direction group.

Next, a regression model was created using each of these three equations to hindcast past significant wave heights for the full duration of the weather record (318 days). Cumulative wave heights were then calculated for each TLS scan interval to investigate the relationship between wave energy and erosion loss as measured by the C2C and M3C2 algorithms. There were a total of 4 TLS scan intervals where interval 1 occurred from February 26, 2015 through March 06, 2015, interval 2 occurred from

February 26, 2015 through April 30, 2015, interval 3 occurred from February 26, 2015 through August 24, 2015, and interval 4 occurred from February 26, 2015 through January 10, 2016.

3.3 Assessing the Importance of Vegetation Roots and Soil Properties on Marsh Edge Erosion

We examined the soil structure and root concentration at the study site to determine how they were correlated with erosion in the marsh. This work was accomplished by creating a voxel model of the root structures from LiDAR data and imagery collected in the marsh. Soil cores were extracted for soil sampling analysis to determine the physical soil properties of the marsh.

3.3.1 Correlation of Roots with Erosion

We sought to correlate the number of roots with erosion using a voxel-based approach. First, the erosion detected by the C2C and M3C3 points for each time interval were combined into a spreadsheet with the point cloud from the initial 0.02 m resolution LiDAR scan (February 2015).

Second, roots and other features were identified in pictures co-referenced with the initial LiDAR scan points. Using ENVI 5.1, regions of interest (ROI) were identified in the imagery and included roots, soil, flare vegetation (flare is sun glare in the imagery that produces high RGB values), and flare soil. The red, green, and blue (RGB) band values of the ROIs were documented.

Third, classification ranges were defined where the selected points from each band had to have brightness values equivalent to 55 to 80, 45 to 85, 48 to 90, or 40 to 90.

The ranges were independently applied to each RGB band and an accuracy assessment was conducted to identify the best range for the roots, soil, and flare ROIs. This assessment showed that the best and most conservative classification required that the RGB values fall between 55 and 80 for all bands simultaneously. This requirement classified the root class at a low and conservative rate of only 14%, though it also minimized the commission error within the soil class (to 2.49%) and two flare classes (to 0%) (Table 1). This requirement was considered optimal because any omitted root point only reduced our overall sample size for the subsequent correlation analysis, while any committed errors with soil or flare points would put errant points into the correlation analysis.

Fourth, a custom script in R Studio 2.1 was utilized to identify the number of root-classified points and the average amount of erosion within each voxel. This analysis was conducted using four sets of voxel sizes, over each of the time intervals: 5 cm x 5 cm, 10 cm x 10 cm, 50 cm x 50 cm, and 100 cm x 100 cm. A regression analysis was conducted for each scale and time interval, where the average erosion was dependent to the number of root points per voxel.

3.3.2 Correlation of Soil with Erosion

Soil cores were collected at five locations every 3 meters along the marsh edge using a specialized 30 x 10 x 10 cm rectangular corer to minimize compaction and sever vegetation roots cleanly [*Feagin* et al., 2009]. Additionally, a soil core sample was collected on the bay bottom of the small cove adjacent to the left edge of the marsh for

Table 1. An accuracy assessment of the February imagery classified using each of the spectral ranges for determining the optimal range to accurately extract the root class.

	55 - 80 RGB Values Band 1		**55 - 80 RGB Values Band 2**		**55 - 80 RGB Values Band 3**		**55 - 80 RGB Values All Bands**	
	% Yes	**% No**	**% Yes**	**% No**	**% Yes**	**% No**	**% Yes**	**% No**
Roots	37.25%	62.75%	38.10%	61.90%	16.68%	83.32%	14.50%	85.50%
Soil	5.94%	94.06%	5.94%	94.06%	2.49%	97.51%	2.49%	97.51%
Flare Soil	14.78%	85.22%	27.83%	72.17%	49.57%	50.43%	0.00%	100.00%
Flare Veg	0.00%	100.00%	0.00%	100.00%	0.23%	99.77%	0.00%	100.00%
	45 - 80 RGB Values Band 1		**45 - 80 RGB Values Band 2**		**45 - 80 RGB Values Band 3**		**45 - 80 RGB Values All Bands**	
	% Yes	**% No**	**% Yes**	**% No**	**% Yes**	**% No**	**% Yes**	**% No**
Roots	64.74%	35.26%	68.53%	31.47%	43.89%	56.11%	39.43%	60.57%
Soil	21.46%	78.54%	31.42%	68.58%	21.07%	78.93%	16.28%	83.72%
Flare Soil	43.48%	56.52%	53.04%	46.96%	57.39%	42.61%	42.61%	57.39%
Flare Veg	0.00%	100.00%	0.00%	100.00%	0.23%	99.77%	0.00%	100.00%
	48 - 90 RGB Values Band 1		**48 - 90 RGB Values Band 2**		**48 - 90 RGB Values Band 3**		**48 - 90 RGB Values All Bands**	
	% Yes	**% No**	**% Yes**	**% No**	**% Yes**	**% No**	**% Yes**	**% No**
Roots	57.06%	42.94%	61.90%	38.10%	34.31%	65.69%	33.36%	66.64%
Soil	16.09%	83.91%	23.56%	76.44%	7.85%	92.15%	7.85%	92.15%
Flare Soil	22.61%	77.39%	43.48%	56.52%	49.57%	50.43%	22.61%	77.39%
Flare Veg	0.00%	100.00%	0.00%	100.00%	1.16%	98.84%	0.00%	100.00%
	40 - 90 RGB Values Band 1		**40 - 90 RGB Values Band 2**		**40 - 90 RGB Values Band 3**		**40 - 90 RGB Values All Bands**	
	% Yes	**% No**	**% Yes**	**% No**	**% Yes**	**% No**	**% Yes**	**% No**
Roots	80.57%	19.43%	84.74%	15.26%	65.12%	34.88%	64.17%	35.83%
Soil	44.44%	55.56%	50.57%	49.43%	31.80%	68.20%	31.80%	68.20%
Flare Soil	67.83%	32.17%	67.83%	32.17%	67.83%	32.17%	67.83%	32.17%
Flare Veg	0.00%	100.00%	0.00%	100.00%	1.16%	98.84%	0.00%	100.00%

comparison. Sampling was conducted on January 10, 2016 after the final TLS scan was acquired.

At collection, cores were sectioned into 5 cm increments and then analyzed for bulk density, percent organic matter, and sediment grain size. Depth segment 1 was at surface level and depth segment 5 was deepest. Samples were first dried at 60 °C for 48 hours and weighed to determine the dry bulk density (g/cm^3). The sample was then incinerated in a furnace for 6 hours at 400°C and reweighed to calculate the percentage of organic matter Lost On Ignition (LOI). Lastly, a grain size analysis was conducted on each post-incineration sample using sieves ranging in size from 0.5 mm to .020 mm. The resulting grain subsets were weighed and standardized by the total weight of the post-incineration sample. The cumulative percentage for each sieve size was then used to calculate mean grain size in phi units (ϕ).

A t-test was calculated to assess differences in the soil metrics between an average of the two cores on the left (cores 1 and 2) and an average of the two cores on the right (cores 4 and 5) at each depth segment of the marsh edge were the TLS scans occurred. The values in core 3 were approximately halfway between those of the two sides and so are not included here.

4. RESULTS

4.1 Terrestrial LIDAR Scanning to Quantify Tidal Marsh Edge Erosion across Temporal and Spatial Scales

The change of each interval was quantified by total average change, average change in the x and y directions, and average change in the z direction. Change in the x and y direction signify horizontal change or, in this specific case, erosion. The majority of change by erosion occurs in the y direction though change also occurs in the x direction as a result of the x-axis not being perfectly perpendicular to the marsh edge. Change in the z direction signifies vertical change, which would measure the marsh edge as well as the height of vegetation at the time of conducting the scan.

Table 2. Average erosion loss results from the M3C2 and C2C algorithms for each interval.

	M3C2 Distance (m)	C2C Absolute Distance (m)	C2C Absolute Distance X (m)	C2C Absolute Distance Y (m)	C2C Absolute Distance Z (m)
Interval 1	-0.081	-0.025	0.004	0.004	-0.002
Interval 2	-0.432	-0.184	-0.082	-0.108	-0.032
Interval 3	-0.903	-0.488	-0.251	-0.323	-0.064
Interval 4	-1.301	-1.095	-0.582	-0.790	-0.160

The C2C method demonstrated a significant rate of erosion at the study site from the February 2015 to January 2016 scans (Table 2). The analysis resulted in 4 C2C analysis change detection clouds – one cloud per interval (Figure 2). During interval 1, the marsh experienced an average loss of 0.025 m in the landward direction, with

average change in the x, y, and z positions at 0.004 m, 0.004 m, and 0.002 m, respectively. During interval 2, the marsh experienced an average loss of 0.184 m with fluctuations in the x, y, and z positions at 0.082 m, 0.108 m, and 0.032 m, respectively. During interval 3, the marsh experienced an average loss of 0.488 m with fluctuations of the x, y, and z positions at 0.251 m, 0.323 m, and 0.064 m, respectively. During interval 4, the marsh experienced an average loss of 1.095 m with fluctuations in the x, y, and z positions at 0.582 m, 0.790 m, and 0.160 m, respectively.

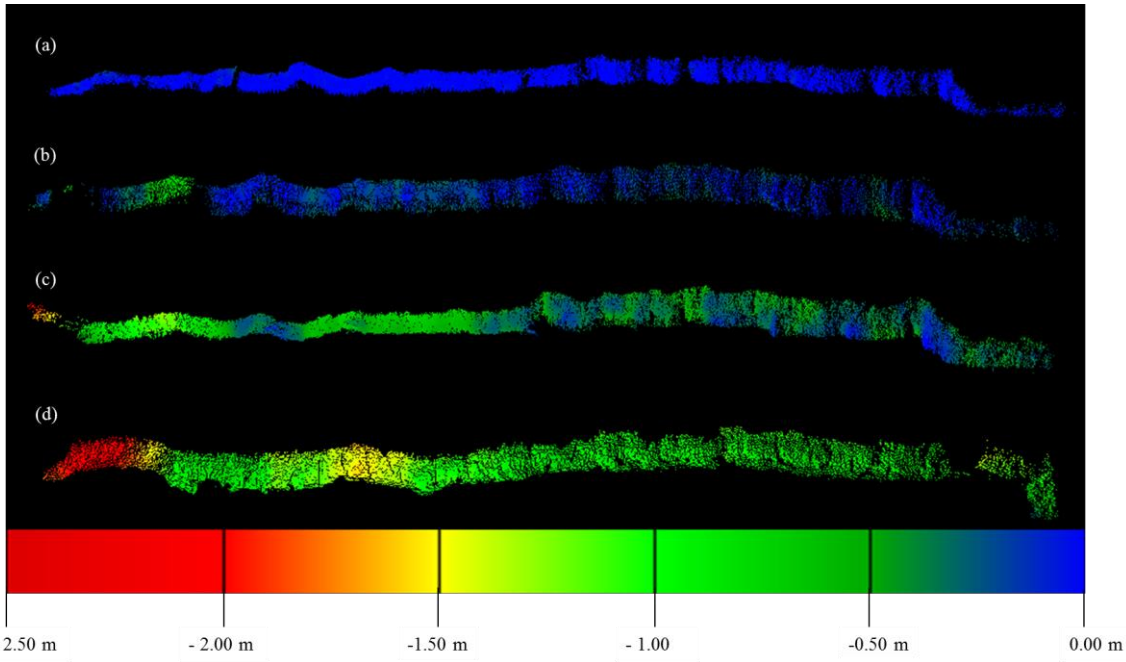

Figure 2. Cloud-to-Cloud (C2C) change analysis results for a) interval 1, b) interval 2, c) interval 3, and d) interval 4.

The M3C2 analysis resulted in 4 change detection clouds – one cloud per interval (Figure 3). The M3C2 method demonstrated significant landward retreat from February 2015 to January 2016. During interval 1, the marsh experienced an average loss of 0.081

m. During interval 2, the marsh experienced an average loss of 0.432 m. During interval 3, the marsh experienced an average loss of 0.903 m. During interval 4, experienced an average loss of 1.301 m.

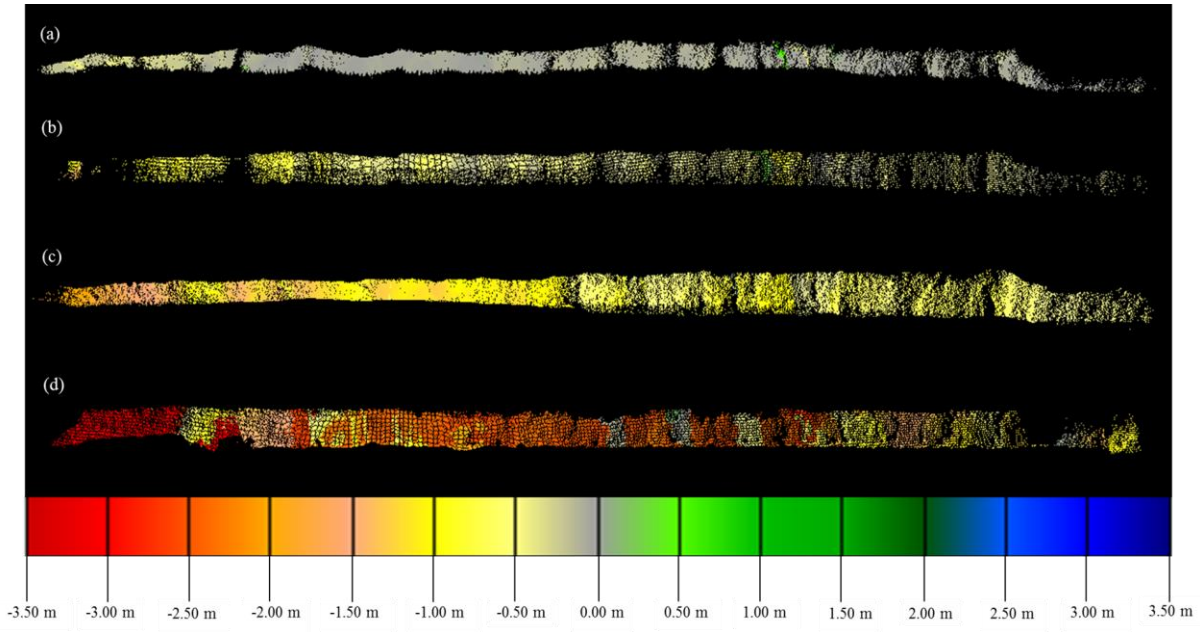

Figure 3. Multi-Model to Model Cloud Comparison (M3C2) change analysis results for: a) interval 1, b) interval 2, c) interval 3, and d) interval 4.

4.2 Correlating Marsh Edge Erosion with Incident Wave Energy

For WDG 1, the significant wave heights were significantly correlated with the wind speed at $p < 0.0001$ and exhibited a good fit at $r^2 = 0.88$. Wave period and wave frequency were also both significantly correlated with wind speed, respectively at $r^2 = 0.75$ and $p < 0.0001$, and $r^2 = 0.79$ and $p < 0.0001$ (Figure 4).

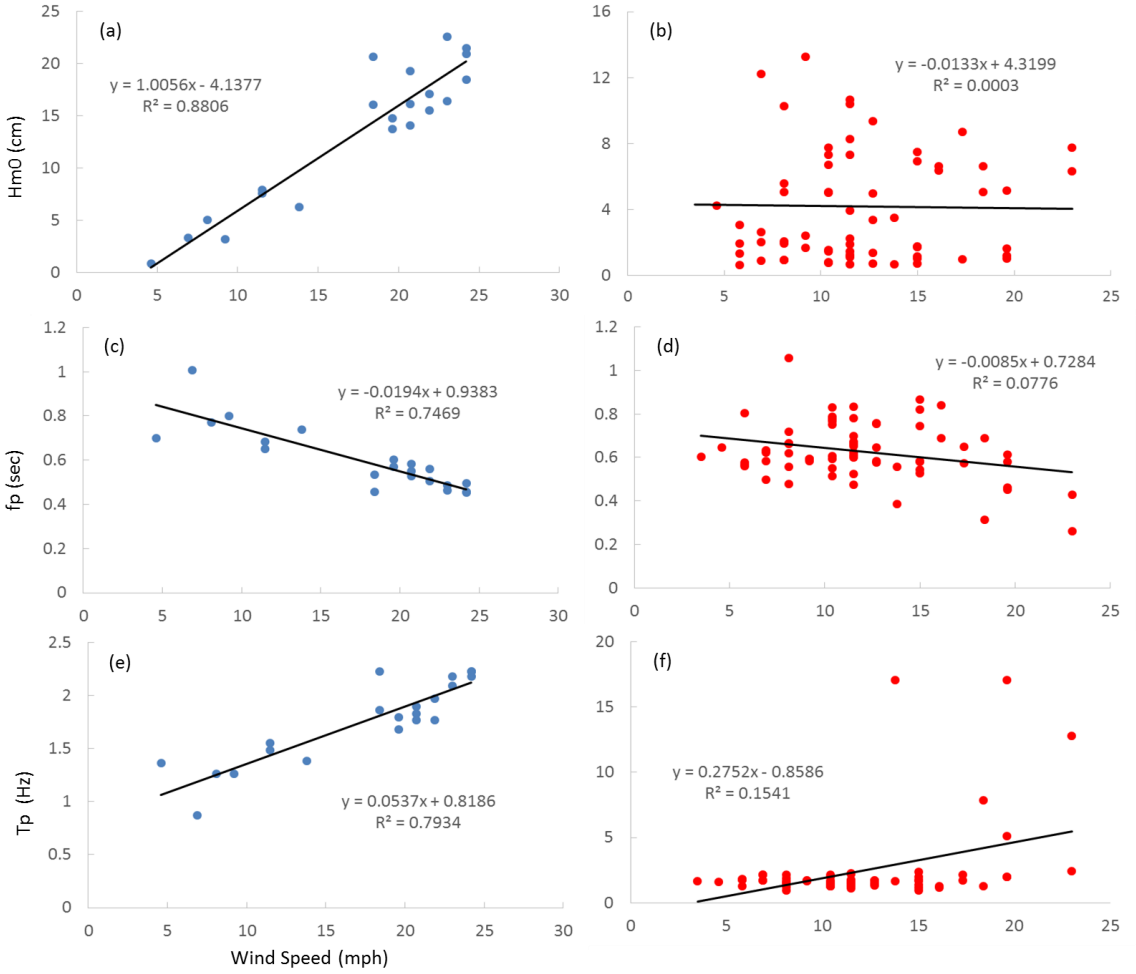

Figure 4. WDG 1 (left column) and WDG 3 (right column) regression analysis for wind speed (independent) versus dependent variables a) and b) significant wave height (Hm0); c) and d) wave period (fp); and e) and f) wave frequency (Tp).

For WDG 2, the significant wave heights were significantly correlated with the wind speed at $p = 0.0002$ and exhibited a good fit at $r^2 = 0.87$. Wave period and wave frequency demonstrated a fair correlation with wind speed, respectively at $r^2 = 0.68$ and $p = 0.0064$, and $r^2 = 0.55$ and $p = 0.0222$.

Lastly for WDG 3, the significant wave heights demonstrated a weak correlation with the wind speed at $p = 0.8950$ and exhibited a poor fit at $r^2 < 0.01$. Wave period and

wave frequency demonstrated a weak correlation with wind speed, respectively at r^2 = 0.08 and p = 0.0235, and r^2 = 0.15 and p = 0.0011.

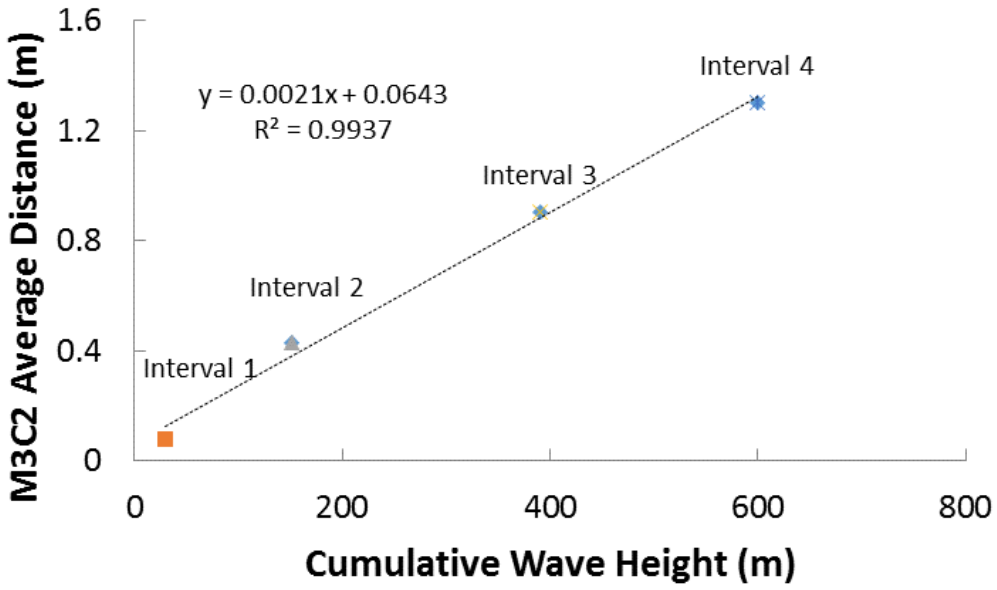

Figure 5. Regression analysis of cumulative wave heights versus M3C2 analysis erosion rates.

For the hindcast model, the cumulative significant wave height within each interval was strongly correlated with the number of days within each interval at r^2 = 0.99. The cumulative significant wave height was well correlated with the C2C total average erosion metric at r^2 = 0.95 and strongly correlated with the M3C2 total erosion metric at r^2 = 0.99 (Figure 5). While this analysis is statistically good, the sample size is small as the regression accounts for only 4 data points.

4.3 Assessing the Importance of Vegetation Roots and Soil Properties on Marsh Edge Erosion

4.3.1 Correlation of Roots with Erosion

Based on the C2C 5 cm x 5 cm voxel analysis results, the influence of root points on erosion for all intervals demonstrated a poor fit at $r^2 = 0.0013$ ($p = 0.6091$), $r^2 = 0.0141$ ($p = 0.0927$), $r^2 = 0.0048$ ($p = 0.3277$), and $r^2 = 0.0654$ ($p = 0.0791$) for each interval respectively (Table 3). At the C2C 10 cm x 10 cm voxel size, the influence of root points on erosion for all intervals demonstrated a poor fit at $r^2 = 0.0084$ ($p = 0.3915$), $r^2 = 0.0066$ ($p = 0.4481$), $r^2 = 0.0002$ ($p = 0.8962$), and $r^2 = 0.1039$ ($p = 0.0934$) for each interval respectively. At the C2C 50 cm x 50 cm voxel size, the influence of root points on erosion for all intervals demonstrated a poor fit at $r^2 = 0.0701$ ($p = 0.4057$), $r^2 = 0.0022$ ($p = 0.8841$), $r^2 = 0.0001$ ($p = 0.0052$), and $r^2 = 0.2090$ ($p = 0.1351$) for each interval respectively. At the C2C 100 cm x 100 cm voxel size, the influence of root points on erosion for all intervals demonstrated a poor fit at $r^2 = 0.0885$ ($p = 0.5171$), $r^2 = 0.0148$ ($p = 0.7953$), $r^2 = 0.0001$ ($p = 0.8775$), and $r^2 = 0.2315$ ($p = 0.2743$) for interval respectively.

Table 3. Regression r^2 and p value results from root voxel C2C analysis.

	Interval 1 C2C		**Interval 2 C2C**		**Interval 3 C2C**		**Interval 4 C2C**	
	r^2	**p value**	**r^2**	**p value**	**r^2**	**p value**	**r^2**	**p value**
5 cm x 5 cm	0.0013	0.6091	0.0141	0.0927	0.0048	0.3277	0.0654	0.0791
10 cm x 10 cm	0.0084	0.3915	0.0066	0.4481	0.0002	0.8962	0.1039	0.0934
50 cm x 50 cm	0.0701	0.4057	0.0022	0.8841	0.0001	0.9902	0.2090	0.1351
100 cm x 100 cm	0.0885	0.5171	0.0148	0.7953	0.0052	0.8775	0.2315	0.2743

Based on the M3C2 5 cm x 5 cm voxel analysis results, the influence of root points on erosion for all intervals demonstrated a poor fit at $r^2 = 0.0032$ ($p = 0.4277$), $r^2 = 0.0032$ ($p = 0.4277$), $r^2 = 0.0093$ (, $p = 0.1742$), and $r^2 = 0.0172$ ($p = 0.0636$) for each interval respectively (Table 4). At the M3C2 10 cm x 10 cm voxel size, the influence of root points on erosion for all intervals demonstrated a poor fit at $r^2 = 0.0051$ ($p = 0.5054$), $r^2 = 0.0051$ ($p = 0.5054$), $r^2 = 0.0168$ ($p = 0.2233$), and $r^2 = 0.0163$ ($p = 0.229$) for each interval respectively. At the M3C2 50 cm x 50 cm voxel size, the influence of root points on erosion for all intervals demonstrated a poor fit at $r^2 = 0.0110$ ($p = 0.7457$), $r^2 = 0.0110$ ($p = 0.7457$), $r^2 = 0.0705$ ($p = 0.4041$), and $r^2 = 0.0576$ (0.4523) for each interval respectively. At the M3C2 100 cm x 100 cm voxel size, the influence of root points on erosion for all intervals demonstrated a poor fit at $r^2 = 0.0322$ ($p = 0.7004$), $r^2 = 0.0322$ ($p = 0.7004$), $r^2 = 0.0655$ ($p = 0.5797$), and $r^2 = 0.0551$ ($p = 0.6124$) for each interval respectively.

Table 4. Regression r^2 and p value results from root voxel M3C2 analysis.

	Interval 1 M3C2		**Interval 2 M3C2**		**Interval 3 M3C2**		**Interval 4 M3C2**	
	r^2	**p value**	**r^2**	**p value**	**r^2**	**p value**	**r^2**	**p value**
5 cm x 5 cm	0.0032	0.4277	0.0032	0.4277	0.0093	0.1742	0.0172	0.0636
10 cm x 10 cm	0.0051	0.5054	0.0051	0.5054	0.0168	0.2233	0.0163	0.2299
50 cm x 50 cm	0.0110	0.7457	0.0110	0.7457	0.0705	0.4041	0.0576	0.4523
100 cm x 100 cm	0.0322	0.7004	0.0322	0.7004	0.0655	0.5797	0.0551	0.6124

4.3.2 Correlation of Soil with Erosion

The average bulk density for all depth segments of the left side of the marsh edge was 0.715 g/cm^3 whereas the right side was 0.654 g/cm^3. The average percent organic matter for all depth segments was 3.04% versus 4.42%, respectively, and the average mean grain size of all depth segments was 2.8ϕ (fine sand) versus 3.03ϕ (very fine sand), respectively.

Bulk density t-test results for a comparison of the side cores versus the right side cores, at depth segments 1 through 5 were 0.0745, 0.119, 0.497, 0.490, and 0.003, respectively. Percent organic matter t-test results for the left versus right side comparison, at depth segments 1 through 5 were 0.106, 0.196, 0.431, 0.365, and 0.177, respectively. Grain size t-test results for left versus right side comparison, at depth segments 1 through 5 were 0.415, 0.415, 0.053, 0.167, and 0.271, respectively. The t-tests results are low as a result of the number core samples used in the calculations.

5. DISCUSSION

5.1 Terrestrial LIDAR Scanning to Quantify Tidal Marsh Edge Erosion across Temporal and Spatial Scales

As measured using the C2C algorithm, the average erosion at the study site for the duration of the study was significant at 1.095 m. When examining the erosion at time interval levels, interval 1 and interval 2 demonstrated minimal retreat at an average distance of less than 0.025 m and 0.18 m, respectively. This was expected because of the short period of 6 days between the baseline scan and the conclusion of interval 1. Interval 2 was also relatively short at 63 days from the baseline scan to its respective conclusion. Greater average erosion was seen during interval 3 and interval 4 with retreat at 0.488 m and 1.095 m, respectively. This erosion also was expected because of the increase in the number of days between the baseline scan and the conclusion of each interval with interval 3 concluding after 179 days and interval 4 concluding after 318 days.

As measured by the M3C2 algorithm, the average landward erosion at the study site for the duration of the study was considerable at 1.301 m. Interval 1 demonstrated the least amount of retreat as expected because of the short interval duration and, as was the case for the C2C analysis, as interval lengths increased so does the average erosion loss at the study site.

The C2C and M3C2 are new cloud-to-cloud analysis methods for direct point cloud comparison. Cloud-to-cloud analysis has been shown to better account for sources

of uncertainty in TLS change detection as compared to surface modeling because it considers the uncertainty caused by point cloud roughness and registration error [*Barnhart and Crosby*, 2013]. While surface modeling comparisons provide good approximations of change, they do not consider local surface orientation of the point cloud and, therefore, cause point cloud displacement calculations to differ depending on point cloud density and surface roughness [*Lague* et al., 2013]. Barnhart and Crosby [2013] conclude the M3C2 algorithm to be the strongest and most versatile point cloud analysis method available as a result of its ability to calculate displacement within a confidence threshold and calculate horizontal displacement, providing a measurement of horizontal erosion rates from point cloud comparisons.

Regardless of the algorithm used for analysis, much erosion can be seen occurring at a rapid rate, with greater than 1 meter of landward erosion occurring in just 318 days. These results are comparable to those of Gibeaut et al. [2003], who calculated an average rate of erosion for the Galveston Bay System at 0.88 m/yr since 1930.

Both algorithm analysis were supported by visually inspecting the study site during TLS field scans, as well as inspecting photographs taken by the TLS scanner. Visual inspection confirmed that the left side of the marsh experienced the majority of the average erosion, and that it was eroding at a faster rate than the right side of the marsh.

The results from each algorithm demonstrate similar rates of erosion; however, the M3C2 algorithm demonstrates slightly higher rates of erosion. This is likely due to the complexity of the algorithm and the user-defined input variables whereas the C2C

algorithm compares each point cloud to one another with minimal user manipulation. The use of these two algorithms is was not intended to be a comparison of their abilities or qualities, but rather, a complete examination of all scenarios that could be occurring at the study site.

5.2 Correlating Marsh Edge Erosion with Incident Wave Energy

Examining the correlation of wind speed and significant wave height within wind direction groups confirmed that wind directions do play a role in erosion retreat in Galveston Bay. The direction of WDG 1 and WDG 2 showed the strongest relationship between wind speed and significant wave height, while the direction of WDG 3 showed a poor relationship between wind speed and significant wave height.

The northeast-southwest orientation of Galveston Island was more significantly impacted by WDG 1 and WDG 2. These wind directions produce larger wave heights that impact the marsh edge and cause more erosion. Winds produced from WDG 1 and WDG 2 push water out of Galveston Bay and into the Gulf of Mexico. In the process, water levels decrease in the bay and greater wave activity is produced, especially where a longer fetch is present. Under these circumstances, waves make impact with the marsh edge at the soil level greatly impacting erosion rates. Whereas, in a contrasting scenario where water levels are higher and waves impact the marsh edge, waves would roll over the soil level and at the vegetation level, therefore, reducing erosion rates. Wind directions from WDG 3 produce this scenario leading to inundation of Galveston Bay and minimal erosion.

The hindcast model revealed several relationships between significant wave heights, days per interval, C2C total average erosion, and M3C2 total average erosion. The strong correlation between significant wave height and number of days per interval serve as validation for the overall usefulness of the hindcast model. Leonardi et al. [2016] support the finding that a linear relationship exists between wave energy and marsh erosion where salt marsh retreat still occurs regardless of how low wave energy conditions become as a threshold below wish no erosion would be expected does not exist. Furthermore, as wave energy increases, salt marshes do not retreat exponentially, emphasizing the resilience of salt marshes against extreme events, because of their short duration [*Leonardi* et al., 2016]. The greatest contributor to salt marsh retreat is moderate, regularly occurring weather conditions [*Leonardi* et al., 2016].

The correlation between cumulative significant wave heights and C2C total average erosion metric, and the M3C2 total average erosion metric suggested that significant wave height drove marsh edge erosion at the study site. Lower amounts of cumulative wave heights were hindcasted for interval 1 and interval 2, which corresponds with the minor erosion calculated by the C2C and M3C2 algorithms in the respective intervals. This was further supported by the minor erosion rates seen firsthand at the study site and documented with photogrammetric images produced from TLS field equipment. Higher amounts of cumulative wave heights were hindcasted for interval 3 and interval 4, which corresponded with the significant erosion calculated by the C2C and M3C2 algorithms in the respective intervals. This also was further

supported by the significant erosion rates seen firsthand at the study site and documented with photogrammetric images produced from TLS field equipment.

5.3 Assessing the Importance of Vegetation Roots and Soil Properties on Marsh Edge Erosion

Overall, the voxel analysis conclusively demonstrated that there was no correlation between erosion and the concentration of roots on the marsh edge, regardless of scale. The presence of roots did not appear to have a significant influence on erosion at the study site.

Marsh retreat occurred at much higher rates on the left side of the marsh, as demonstrated by TLS data analysis. Correspondingly, the left side of the marsh had a higher volume of bulk density, a lower percentage of organic matter, and on average a larger grain size as compared to the right side of the marsh. Salt marsh resistance to wave erosion is tied to local properties such as characteristics of the sediments [*Leonardi* et al., 2015]. Soil composition likely contributed to the observed left-versus-right erosion patterns, as Feagin et al. [2009] linked each of these three factors with increased erosion for soils within the same region. When examining each depth segment, the bulk density and percent organic matter were most different between the left and right sides of the marsh at depth segments 3 and 4, roughly 15 -20 cm deep. The soil properties transition at this depth because fluctuating sea level rise during the last half century altered vegetation cover and associated organic sediment accumulation rates at our study site [*Kulawardhana* et al., 2015]. Erosion is driven by wave impact and shear at this depth transition point in soils from [*Feagin* et al. 2009], and this could potentially explain why

soil differences in the left versus right side of the marsh were associated with similar erosion patterns.

6. SUMMARY AND CONCLUSIONS

Overall, lateral marsh edge erosion at the study site for the duration of the study was relatively large. The marsh edge is eroding at a rapid rate and is demonstrated by the interval change detection results from multiple methods of analysis. An average of over 1 meter of erosion was observed at the study site in a 318 day period.

Causes of the marsh edge erosion could be many; however, we examined the significance of incident wave energy, vegetation root concentration, and marsh soil properties. Wind direction, when coupled with wind speed and significant wave height, plays a factor in erosion at the study site. The orientation of Galveston Island makes it prone to greater erosion when winds blow from the east-northeast to the north directions and from the north-northwest to the west directions. The direction of these winds push water out of Galveston Bay and into the Gulf of Mexico; the decreased water levels in combination with greater wave activity have a significant impact on the amount of erosion in the marsh.

While root concentration did not play a significant role in erosion prevention, soil properties appeared to have some influence. Other factors not included in this study that could play a role in the rapid retreat of the study site could include human impact from the use of recreational watercraft, the wave energy created by watercraft, or the bathymetry of Galveston Bay.

As exemplified by the marsh study site in Galveston Bay, marsh erosion is occurring quite rapidly over time. Many of Galveston Island's marshes will likely see

similar losses over time, leaving a grim outlook for these areas which are an essential transition zone from aquatic to terrestrial ecosystems and provide numerous ecosystem goods and services.

REFERENCES

Barnhart, T., and B. Crosby (2013), Comparing two methods of surface change detection on an evolving thermokarst using high-temporal-frequency terrestrial laser scanning, Selawik River, Alaska, *Remote Sensing*, 5, 2813 -2837.

Cahoon, D. R., P. Hensel, J. Rybczyk, K. L. McKee, C. E. Proffitt, and B. C. Perez (2003), Mass tree mortality leads to mangrove peat collapse at Bay Islands, Honduras after Hurricane Mitch, *Journal of Ecology*, 91(6), 1093 - 1105.

Fagherazzi, S., and P.L. Wiberg (2009), Importance of wind conditions, fetch, and water levels on wave-generated shear stresses in shallow intertidal basins, *Journal of Geophysical Research Earth Surface*, 114, F03022.

Feagin, R. A., S. M. Lozada-Bernard, T. M. Ravens, I. Moller, K. M. Yeager, and A. H. Baird (2009), Does vegetation prevent wave erosion of salt marsh edges?, *PNAS*, 106(25), 10109 - 10113.

Feagin, R. A., A. M. Williams, S. Popescu, J. Stukey, and R. A. Washington-Allen (2014), The use of terrestrial laser scanning (TLS) in dune ecosystems: The lessons learned, *Journal of Coastal Research*, 30, 111 - 119.

Francalanci, S., M. Bendoni, M. Rinaldi, and L. Solari (2013), Ecomorphodynamic evolution of salt marshes: Experimental observations of bank retreat processes, *Geomorphology*, 195, 53 - 65.

French, J. R., and H. Burningham (2009), Coastal geomorphology: trends and challenges, *Progress in Physical Geography*, 33(1), 117 - 129.

Gibeaut, J. C., R. Waldinger, T. Hepner, T. A. Tremblay, and W. A. White (2003), Changes in West Bay Shoreline Position, West Bay System, Texas, Bureau of Economic Geology: Austin, Texas.

Glass, P., and T. Hollingsworth (1999), Wetlands restoration at Galveston Island State Park a multi-agency project, in Proceedings of the Galveston Bay Estuary Program State of the Bay Symposium IV, pp. 203-204, Galveston, Texas.

Guarnieri, A., A. Vettore, F. Pirotti, M. Menenti, and M. Marani (2009), Retrieval of small-relief marsh morphology from terrestrial laser scanner, optimal spatial filtering, and laser return intensity, *Geomorphology*, 113, 12 - 20.

Hackney, C., S. E. Darby, and J. Leyland (2015), Landscapes on the edge: examining the role of climatic interactions in shaping coastal watersheds using a coastal-terrestrial landscape evolution model, *Earth Surface Processes and Landforms*, 40, 313 - 325.

Hoffmeister, D., N. Tilly, C. Curdt, H. Aasen, K. Ntageretzis, H. Hadler, T. Willershauser, A. Vott, and G. Bareth (2012), Terrestrial laser scanning for coastal geomorphologic research in Western Greece, *International Archives of the Photogrammetry, Remote Sensing and Spatial Information Sciences*, 39(B5), 511 - 516.

Hopkinson, C., L. Chasmer, C. Young-Pow, and P. Treitz (2004), Assessing forest metrics with a ground-based scanning lidar, *Canadian Journal of Forest Research*, 34, 573 - 583.

Houser, C. (2010), Relative importance of vessel-generated and wind waves to salt marsh erosion in a restricted fetch environment, *Journal of Coastal Research*, 26(2), 230 - 240.

Karimpour, A. (2015), OCEANLYZ, Ocean Wave Analyzing Toolbox, user manual, http://www.arashkarimpour.com/download.html.

Kulawardhana, R. W., R. A. Feagin, S. C. Popescu, T. W. Boutton, K. M. Yeager, and T. S. Bianchi (2015), The role of elevation, relative sea level history and vegetation transition in determining carbon distribution in *Spartina alterniflora* dominated salt marshes, *Estuarine, Coastal and Shelf Science*, 154, 48 - 57.

Lague, D., N. Brodu, and J. Leroux (2013), Accurate 3D comparison of complex topography with terrestrial laser scanner: Application to the Rangitikei canyon (N-Z), *ISPRS Journal of Photogrammetry and Remote Sensing*, 82, 10 - 26.

Leonardi, N., N. K. Ganju, and S. Fagherazzi (2016), A linear relationship between wave power and erosion determines salt-marsh resilience to violent storms and hurricanes, *PNAS*, 113(1), 64 - 68.

Leonardi, N., and S. Fegherazzi (2015), Effect of local variability in erosion resistance on large-scale morphodynamic response of salt marshes to wind waves and extreme events, *Geophysical Research Letters*, 42(14), 5872 - 5879.

Leonardi, N., and S. Fegherazzi (2014), How waves shape salt marshes, *Geological Society of America*, 42(10), 887 - 890.

Marani, M., A. D'Alpaos, S. Lanzoni, and M. Santalucia (2011), Understanding and predicting wave erosion of marsh edges, *Geophysical Research Letters*, 38(L21401), 1 - 5.

Mori, N., T. Suzuki, and S. Kakuno (2007), Noise of acoustic Doppler velocimeter data in bubbly flows, *Journal of Engineering Mechanics*, 133(1), 122 - 125.

Olsen, M., E. Johnstone, N. Driscoll, S. Ashford, and F. Kueste (2009), Terrestrial laser scanning of extended cliff sections in dynamic environments: Parameter analysis, *Journal of Surveying Engineering*, 161 - 169.

Pirotti, F., A. Guarnieri, and A. Vettore (2011), Vegetation characteristics using multi-return terrestrial laser scanner, *International Archives of the Photogrammetry, Remote Sensing and Spatial Information Sciences*, 38(W12), 277 - 282.

Ravens, T. M., R. C. Thomas, K. A. Roberts, and P. H. Santschi (2009), Causes of salt marsh erosion in Galveston Bay, Texas, *Journal of Coastal Research*, 25(2), 265 - 272.

Roth, D. (2010), Texas hurricane history, National Weather Service: Camp Springs, MD.

Ryding, J., E. Williams, M. Smith, and M. Eichhorn (2015), Assessing handheld mobile laser scanners for forest surveys, *Remote Sensing*, 7, 1095 - 1111.

Schubert, J. E., T. W. Gallien, M. S. Majd, and B. F. Sanders (2015), Terrestrial laser scanning of anthropogenic beach berm erosion and overtopping, *Journal of Coastal Research*, 31, 47 - 60.

Schwimmer, R. A. (2001), Rates and processes of marsh shoreline erosion in Rehoboth Bay, Delaware, USA, *Journal of Coastal Research*, 17(3), 672 - 683.

Shafer, D. J., R. Roland, and S. L. Douglass (2003), Preliminary evaluation of critical wave energy thresholds at natural and created coastal wetlands, WRP Technical Notes Collection (ERDC TN-WRP-HS-CP-2.2), U.S. Army Engineer Research and Development Center: Vicksburg, Mississippi.

Silliman, B. R., J. van de Koppel, M. W. McCoy, J. Diller, G. N. Kasozi, K. Earl, P. N. Adams, and A. R. Zimmerman (2012), Degradation and resilience in Louisiana salt marshes after the BP–Deepwater Horizon oil spill, *PNAS*, 109(28), 11234 - 11239.

Silva dos Santos, A. L., V. E. Amaro, and M. S. T. Santos (2014), Terrestrial Laser Scanner Applied to Monitoring Beach Morphological Changes in a High Energy Coastal Zone in Northeast Brazil, *Conference: 7th International Terrestrial Laser Scanner user meeting in Rome, Italy.*

Teal, J. M. (1962), Energy Flow in the salt marsh ecosystem of Georgia, *Ecology*, 43(4), 614 - 624.

van der Wal, D., and K. Pye (2004), Patterns, rates and possible causes of saltmarsh erosion in the Greater Thames area (UK), *Geomorphology*, 61, 373 - 391.

White, W. A., and R. A. Morton (1997), Wetland losses related to fault movement and hydrocarbon production, southeastern Texas coast, *Journal of Coastal Research*, 13(4), 1305 - 1320.

White, W. A., R. A. Morton, and C. W. Holmes (2002), A comparison of factors controlling sedimentation rates and wetland loss in fluvial-deltaic systems, Texas Gulf coast, *Geomorphology*, 44, 47 - 66.

White, W. A., T. A. Tremblay, E. G. Wermund, Jr., and L. R. Handley (1993), Trends and status of wetlands and aquatic habitats in the Galveston Bay System, Texas, GBNEP-31, Galveston Bay National Estuary Program Publication: Webster, Texas.